Ionics
https://doi.org/10.1007/s11581-021-04233-4

ORIGINAL PAPER

A fluorescent probe for selective detection of Fe^{3+} by using a self-assembled nitrogen-doped carbon quantum dots-3,4,9,10-perylenetetracarboxylic acid composite

Kunjie Wang[1] · Jinliang Chen[1] · Hongxia Li[1] · Mengmeng Zhang[1] · Quanxing Liao[1] · Letong Wang[1] · Yuhua Zhang[1] · Xiaohui Niu[1]

Received: 30 April 2021 / Revised: 28 June 2021 / Accepted: 12 August 2021

Abstract

We have synthesized nitrogen-doped carbon quantum dots (N-CQDs) via one-step hydrothermal method by using citric acid and urea as carbon sources, In order to solve the agglomeration effect of carbon quantum dots and increase its recognition sites, and then combined the N-CQDs with 3,4,9,10-perylenetetracarboxylic acid (PTCA) to synthesize an self-assembled carbon quantum dots-3,4,9,10-perylenetetracarboxylic acid (N-CQDs/PTCA) composite, which has strong fluorescent properties. The fluorescence spectrum showed that the prepared self-assembled composite (N-CQDs/PTCA) has strong yellow-green light emission near 510 nm. The characterizations such as ultraviolet–visible absorption, X-ray electron spectroscopy, Fourier infrared spectroscopy, and transmission electron microscopy have confirmed that the N-CQDs and PTCA were combined together successfully. And the prepared self-assembled N-CQDs/PTCA was independent of excitation. It has stable and strong fluorescence properties and can be used as a fluorescent probe. The study also found that in the presence of Fe^{3+} ions, the fluorescence of self-assembled carbon quantum dots N-CQDs/PTCA will be quenched, and the quenching efficiency had a good linear relationship with the concentration of Fe^{3+} ions. Therefore, we proposed to use the self-assembled carbon quantum dots N-CQDs/PTCA as a fluorescent probe to detect Fe^{3+} selectively. The results showed that the method was fast, reliable, obvious detection signal, selective, and not affected by incubation time. The detection limit is 0.041 μM, which provides a new idea for the detection of Fe^{3+} ions by using self-assembled method and has broad application prospects.

Keywords Carbon quantum dots · PTCA · Fluorescent probe · Ferric ion

Introduction

With the development of nanomaterials in recent years, more and more nanomaterial probes with excellent properties have been developed, especially the carbon quantum dots probe. The carbon quantum dots combine a variety of advantages such as small size, high luminous efficiency, strong light stability, simple preparation, adjustable luminescence color, easy functional modification, low cytotoxicity, good water solubility, and biocompatibility. The series of the advantages carbon quantum dots provide unprecedented opportunities for biological imaging and sensing [1]. Carbon dots (CDs), also known as carbon quantum dots (CQDs), are monodisperse quasi-spherical carbon nanoparticles with a core–shell structure, which has a particle size of less than 10 nm. Due to its special structure and quantum size effect, dielectric confinement effect, and surface effect, carbon quantum dots have a wide excitation range, narrow emission peak and large Stokes shift [2]. Changes in carbon sources, experimental conditions, and functional groups can result in different properties [3], such as water solubility and biocompatibility. In recent years, carbon quantum dots have shown broad applications prospects in metal ion detection [4–6], bioimaging [7–9], photocatalysis [10], light-emitting devices [11], medicine [12], and DNA detection [13].

The detection of small and macromolecules with a first, convenient, sensitive, and cost-effective physical and environmental is essential in the biological, clinical, environmental, and industrial fields [14, 15]. For example, iron (Fe), and one of the most basic elements in biological

✉ Kunjie Wang
wangkj80@163.com

[1] College of Petrochemical Technology, Lanzhou University of Technology, 730050 Lanzhou, People's Republic of China

Published online: 24 August 2021

systems, is the fourth most abundant element in the earth's crust (calculated by weight). It is an essential micronutrient for the human body, which carries part of oxygen and constitutes hemoglobin, myoglobin, and enzymes [16]. The iron content of natural water depends on the other chemical composition of the geological area and waterways. Fe^{3+} ions are the most important form of pollution in the water environment [17, 18]. In nature, iron usually exists in the form of soluble Fe^{3+} ions. Excessive Fe^{3+} is a potential health hazard. The unbalanced regulation of Fe^{3+} content can lead to anemia, Alzheimer's disease, Parkinson's disease, mental decline, hemochromatosis, diabetes, and cancer [17, 19]. Therefore, the detection of Fe^{3+} has great prospects for the early diagnosis of these diseases. Typical technologies for Fe^{3+} detection include plasma emission spectroscopy [20] and colorimetry [21]. However, these methods are complicated and expensive, and the detection is limited by the accuracy of the instrument. Compared with the instrument method, the optical method has a lower cost, which is a more economical method [22, 23]. Among them, fluorescence sensing has the advantages of simple operation, fast, fast real-time monitoring, and high sensitivity [24, 25]. It is a new method for fast and easy detection of metal ions [26–28]. Therefore, it is necessary to design a simple, cheap, sensitive, selective, and easy-to-operate method to detect Fe^{3+} [29, 30].

3, 4, 9, 10-perylenetetracarboxylic acid (PTCA) is a 5-ring polycyclic aromatic hydrocarbon rich in carboxyl groups, which has a large π-π conjugated system [31, 32]. Among them, PTCA provides a large platform to support the formation of stable amide bonds between carbon quantum dots and carboxyl groups in PTCA [33, 34], so that carbon quantum dots and PTCA can compound to form the complex of carbon quantum dots, reducing the agglomeration effect of carbon quantum dots and increasing the recognition sites. In addition, it can be clearly seen from the UV lamp that the combination of the two increases the light intensity of the carbon dots to a certain extent and makes them stable.

In this study, citric acid and urea are used as carbon sources to synthesize nitrogen-doped carbon quantum dots (N-CQDs), and then combine with PTCA to N-CQDs/PTCA with high fluorescence and stability. The result shows that it has the advantages of high water solubility and non-toxicity of carbon quantum dots while maintaining a stable and strong fluorescence. The method is simple, economical, one-step hydrothermal, and the N-CQDs/PTCA has strong yellow-green light emission at about 510 nm. We characterized the structure of the prepared composite and studied the fluorescence properties of the composite in the presence of metal ions. The results show that the fluorescence of the complex can be selectively quenched by Fe^{3+} ions, and the fluorescence quenching rate has a good linear relationship with the concentration of Fe^{3+} ions at the range of 20 to 60 μM. Therefore, we have established a fluorescence method for selective detection of Fe^{3+} ions using N-CQDs/PTCA. This method has high accuracy, good selectivity, and strong fluorescence intensity. Besides, the detection signal is more obvious, which provides potential practical applications for environmental analysis.

Experimental section

Instruments and chemicals

X-ray diffractometer (model) was used to record XRD patterns in the range of 5.0 to 80.0° at a scan rate of 5.0°/min. Fourier transform infrared spectroscopy (FTIR) (Nicolet AVTAR360) was used to identify the surface groups of freeze-dried N-CQDs and N-CQDs/PTCA at a wavelength of 4000–500 cm^{-1}. X-ray photoelectron spectroscopy (XPS) (D8 Advance) scanning electron microscope (SEM) (Ultra Pius) and transmission electron microscope (TEM) (FEI TECNAI G2 F20) were used to study the size and morphology of the synthesized N-CQDs and N-CQDs/PTCA. The fluorescence spectrum was measured with a FluoroMax-4 (HORIBA, USA) fluorescence spectrophotometer. The photos for visual fluorescence were taken with a mobile phone iphone11, and a PHS-25 acidity meter (Shanghai Thunder Magnetic Instrument Factory, China) was used to prepare different pH solutions.

Citric acid (CA), urea (analytical grade), and 3,4,9,10-perylenetetracarboxylic acid (PTCA) were purchased from Aladdin (Shanghai, China), while hydrochloric acid (HCl), $FeCl_3$, $CaCl_2$, $MgCl_2$, $AlCl_3$, ZnCl, MnCl, LiCl, $CuCl_2$, $CdCl_2$, NaCl, CoCl, CrCl, NiCl, $BaCl_2$, KCl, and $FeCl_2$ were purchased from Sinopharm Holding Co., Ltd. (Shanghai, China), and ultrapure water was used to prepare all solutions.

Preparation of N-CQDs

The carbon quantum dots were synthesized by a simple hydrothermal method. 2.52 g of citric acid and 2.16 g of urea was added into a 100-mL beaker, then add 60 ml of deionized water. The obtained solution was stirred with a glass rod to completely dissolve the citric acid and urea, which was added in a 100-mL hydrothermal kettle and reacted 160 °C for 4 h. After being naturally cooled to room temperature, the sample and absolute ethanol were allowed to stand for 24 h at a ratio of 5:1, then dialyzed for 72 h and then taken out and freeze-dried.

Preparation of PTCA and N-CQDs/PTCA

0.5 g PTCA was dissolved in 50 mL 0.1 M NaOH. Then it was stirred vigorously until the red color turns yellow-green. 1.0 M HCl was added dropwise to make it completely precipitate. The precipitate was further filterred with a 0.2-μm microporous membrane. Finally, the product was put in freeze drying equipment.

The prepared 40 mg N-CQDs and 20 mg PTCA were put in a 100-mL beaker at a ratio of 2:1, then added 20 mL of deionized water and sonicated for 2 h to fully dissolve. The obtained solution was added into a 100-mL round-bottomed flask in an oil bath with reaction temperature kept at 40℃. The reaction was stirred for 24 h. Finally, the obtained product was filtered with a 0.2-μm microporous membrane, and the upper layer of the precipitate was taken and freeze-dried to obtain N-CQDs/PTCA.

Results and discussion

Structural characterization of N-CQDs/PTCA

As shown in Fig. 1a, the TEM image of N-CQDs shows that it has good monodispersity and a relatively narrow size distribution. According to the illustration, it can be seen that the particle size of N-CQDs is about 2.2 nm. The above results show the pure and impurity-free nitrogen-doped carbon quantum dots. We can see from the SEM image of N-CQDs /PTCA (Fig. 1b) that N-CQDs /PTCA composite material presents a highly porous structure and a uniformly lamellar morphology. We can infer that this composite material has good dispersivity and can increase the recognition sites of the composite material, so PTCA and N-CQDs are combined together to improve the agglomeration effect.

As shown in Fig. 2a, N-CQDs have two characteristic absorption peaks, one is a strong absorption peak at 335 nm, which may be caused by the π-π* transition of sp^2 carbon atoms, and the other is a weak absorption peak at 600 nm. It is produced by the n-π* transition of the C = O bond. When PTCA and N-CQDs are compounded together, N-CQDs/PTCA have a strong absorption peak at 460 nm, which may be caused by the n-π* transition of C = O bond. The absorption band of N-CQDs/PTCA has a large overlap with its emission. Therefore, based on the unique and coordinated carbon quantum dot complex N-CQDs/PTCA, an effective FRET-based fluorescence sensing platform can be established. In order to prove the successful synthesis of N-CQDs/PTCA composite materials, we have tested the FT-IR spectra of N-CQDs, PTCA, and N-CQDs/PTCA and performed a detailed analysis. As shown in Fig. 2b, the peak at 3419 cm^{-1} and the peak at 1774 cm^{-1} are designated as the stretching vibrations of the O–H bond and C = O bond. Because N-CQDs contain –NH, the bending vibration peak of –NH appears at 1560 cm^{-1} of N-CQDs and N-CQDs/PTCA, and the stretching vibration of C–O–C appears at 1130 cm^{-1} of PTCA and N-CQDs/PTCA, so the FT-IR results confirmed the successful combination of N-CQDs and PTCA. Further characterization was performed by the XRD pattern of N-CQDs, PTCA, and N-CQDs/PTCA. Figure 2c shows that N-CQDs have an amorphous diffraction peak at 2θ of 27°, which is consistent with the XRD pattern of carbon quantum dots in the previous literature [35, 36]. In the comparison of XRD images of PTCA and N-CQDs/PTCA, the diffraction peaks of PTCA also existed in N-CQDs/PTCA, which confirmed that N-CQDs and

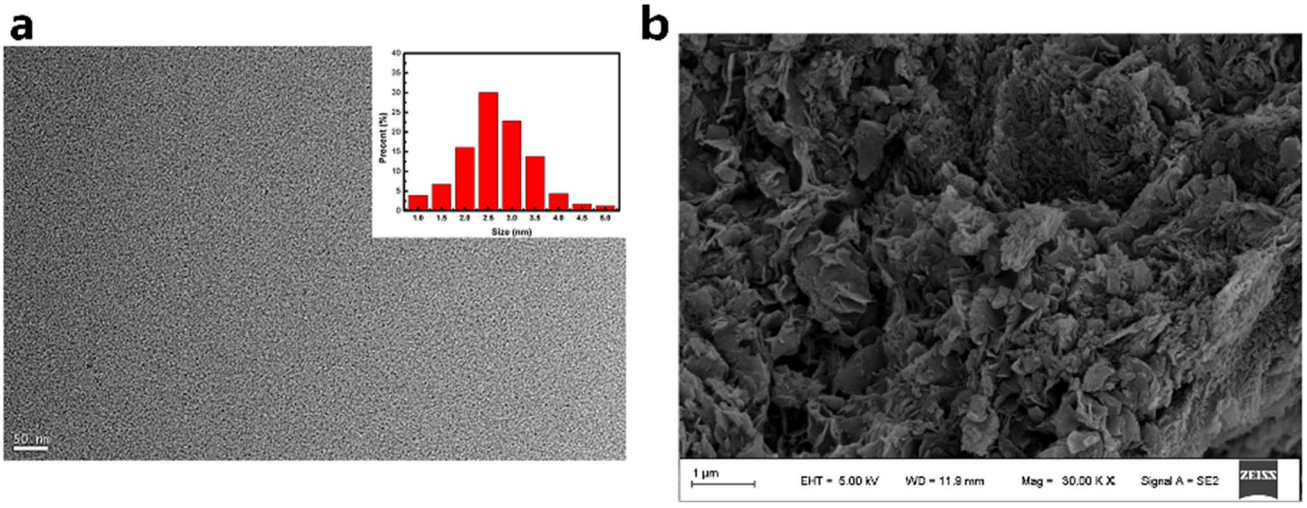

Fig. 1 **a** TEM images of pure N-CQDs; (Insert in (**a**) was size distribution (statistics: 100 measurements from TEM image) of CQDs). **b** SEM images of N-CQDs/PTCA

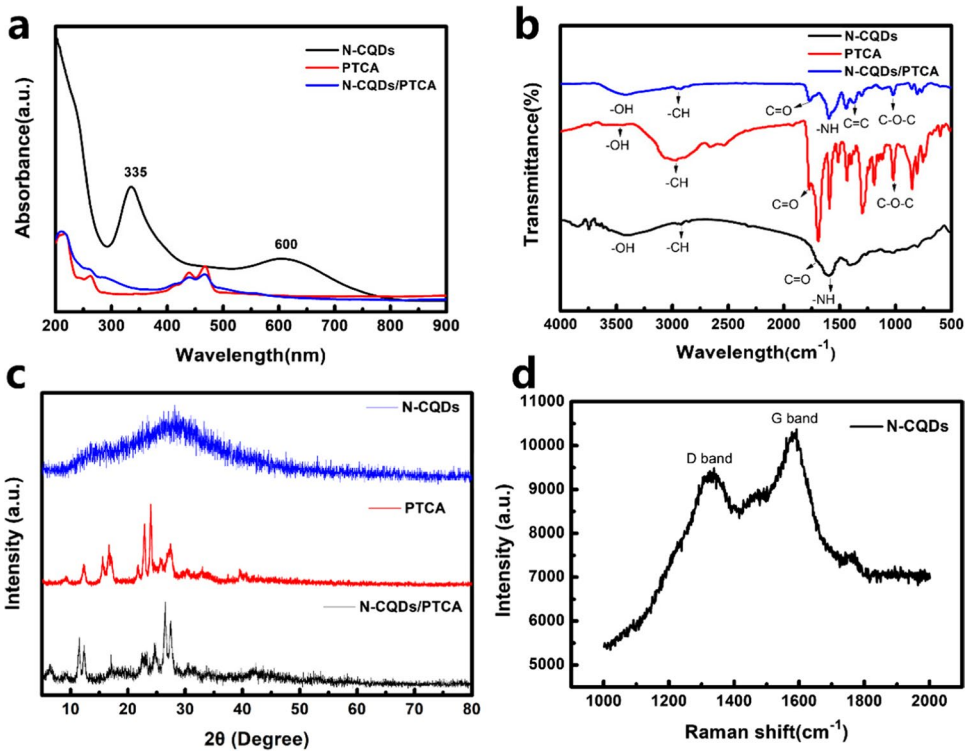

Fig. 2 **a** N-CQDs Raman spectroscopy. **b** N-CQDs, PTCA and N-CQDs/PTCA UV-visible-absorption spectrum, **c** FT-IR spectra of N-CQDs, PTCA and N-CQDs/PTCA, **d** XRD-spectra of N-CQDs, PTCA and N-CQDs/PTCA

PTCA were combined together. In addition, the Raman spectra of N-CQDs showed two characteristic peaks at 1325 and 1580 cm^{-1}, which belonged to the **D** band and **G** band, respectively. The I_D/I_G intensity ratio of N-GQDs is 0.84. The strength of the **G** band is higher than that of the **D** band, indicating that the composition of crystalline graphite is greater than that of amorphous carbon, which can also prove the successful preparation of N-CQDs [36].

XPS spectrum can be used to study the element composition and chemical state of N-CQDs/PTCA. The results of the XPS survey spectrum (Fig. 3a) show that N-CQDs/PTCA contains C, O, and N four elements, the contents of which are 74.94%, 22.73%, and 2.33%, respectively. XPS investigation of N-CQDs/PTCA shows that there are three peaks at 284.81 eV, 531.87 eV, and 400.17 eV, proving the existence of C 1 s, O 1 s, and N 1 s respectively. The C 1 s spectrum (Fig. 3b) is divided into 3 peaks at 284.8 eV, 288.5 eV, and 285.1 eV, which are attributed to C–C (sp^3)/C = C (sp^2), O–C = O (sp^2), and C–N. The O 1 s spectrum (Fig. 3c) can be divided into three peaks, corresponding to C = O at 531.75 eV, C–OH/C–O–C at 533.2 eV, and O–C = O at 530.5 eV. The N 1 s spectrum (Fig. 3d) can be divided into two peaks, where the peak of N–H is at 400.55 eV and the peak of C–N is at 399.66 eV. The –NH in the N-CQDs is also proved in the N-CQDs/PTCA. According to the above results, the successful recombination of N-CQDs and PTCA is also proven.

According to the nitrogen isothermal adsorption and desorption curve of N-CQDs/PTCA (Fig. 4a), it belongs to the H3 type hysteresis bad isotherm, without obvious saturation adsorption platform, and the pore structure is not very regular. The pore size distribution diagram of N-CQDs/PTCA (Fig. 4b) shows that the pore size distribution of the prepared composites is basically between 10 and 20 nm, and surface area is 273.73 m^2/g, further proving that which is mesoporous carbon material. It has good thermal stability and hydrothermal stability and can be used in biosensors.

According to the TGA curve of N-CQDs (Fig. 5), it can be clearly seen that at the initial temperature, the weight loss content exceeded 100% due to the addition of N_2, and then with the increase of temperature, water was volatilized after 100 °C, so the curve began to decline slowly. When the temperature reaches 200 °C, because of the weakening of π-π bonding force, C = O and $–NH_2$ generate CO_2, H_2O, and N_2, and the weight also begins to drop sharply. When the temperature reaches 600 °C, the fracture of the carbon skeleton begins to occur, and the carbon quantum dots turn into carbon black. Finally, when the temperature reaches 800 °C, the weight loss of N-CQDs reaches 25%. TGA curve of PTCA showed that the addition of N_2 at the beginning of the curve, weightlessness content more than 100%; but water is volatile when after 100 °C, curve began to fall, and after 450 °C C–O–C, –COOH formation of CO_2 and H_2O in curve fell sharply, after 600 °C fracture, begin with the carbon skeleton into carbon black, eventually PTCA at 800 °C the weightlessness of up to 15%. However, when PTCA is compounded to carbon quantum dots, according to the TGA curve of N-CQDs/PTCA, it can be seen that its

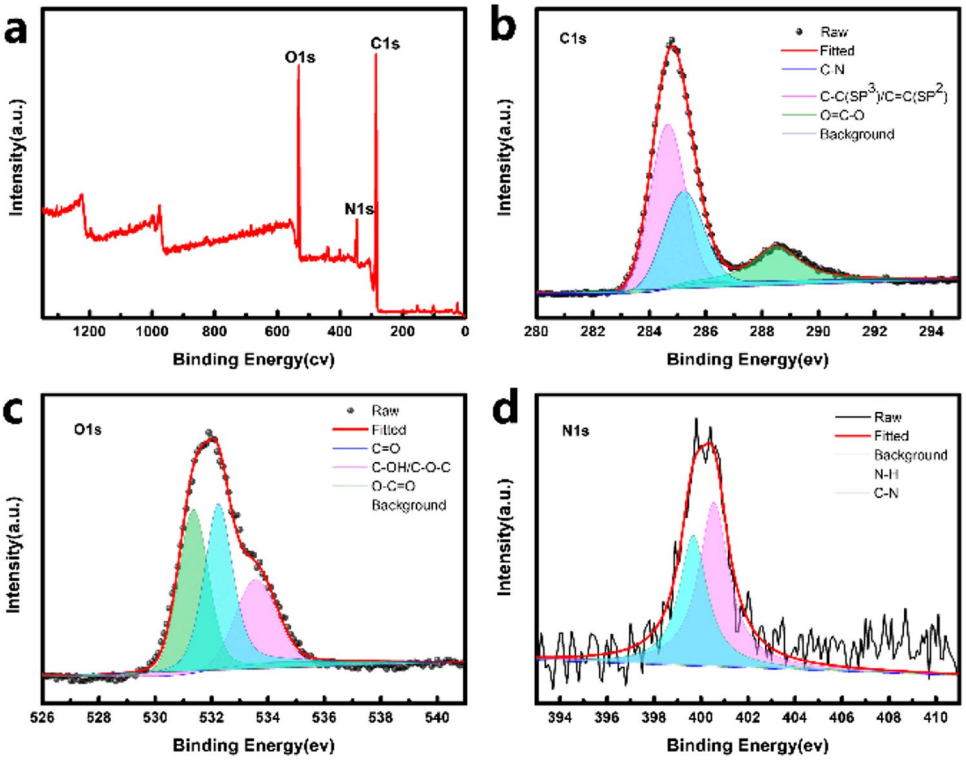

Fig. 3 **a** XPS survey spectrum; **b** High-resolution C1s peaks and fitting curves; **c** High-resolution O1s peaks and fitting curves; **d** High-resolution N1s peaks andfitting curves

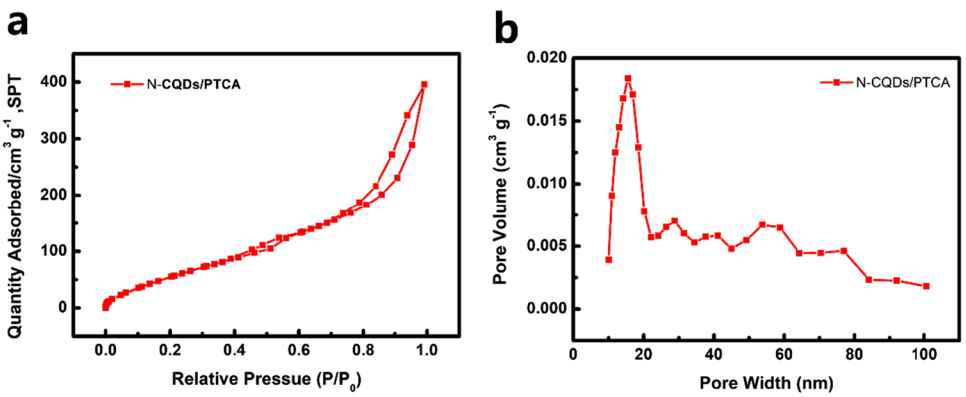

Fig. 4 **a** Nitrogen isothermal adsorption and desorption curve of N-CQDs/PTCA; **b** pore size distribution diagram

thermal stability is the best, and the weight loss at 800 °C is only 61%. Due to the hydrogen bond between N-CQDs and PTCA and the π-π transition, the interfacial adhesive force is improved, so the thermal stability of N-CQDs is greatly increased. This result also proves the successful combination of PTCA and N-CQDs.

N-CQDs/PTCA optical properties

In order to explore its optical properties, we found its maximum excitation and emission wavelengths at 460 nm and 510 nm in the fluorescence spectrum (Fig. 6a). The photoluminescence (PL) behavior of N-CQDs/PTCA under different excitation wavelengths was studied. As shown in Fig. 6b, the fluorescence intensity also increases rapidly as the excitation wavelength increases from 370 to 460 nm. However, the fluorescence intensity drops rapidly, reaching a peak at 460 nm as the excitation wavelength increases from 460 to 480 nm. In addition, most of the carbon quantum dots and their complexes have a red shift in the PL peak with the increase of the excitation wavelength, but the N-CQDs/PTCA does not show a more obvious red shift. The above results show that when PTCA is compounded on the carbon quantum dots, its surface defects are changed, thereby showing PL characteristics independent of excitation, indicating that the synthesized N-CQDs/PTCA is uniform and stable and has strong fluorescence characteristics.

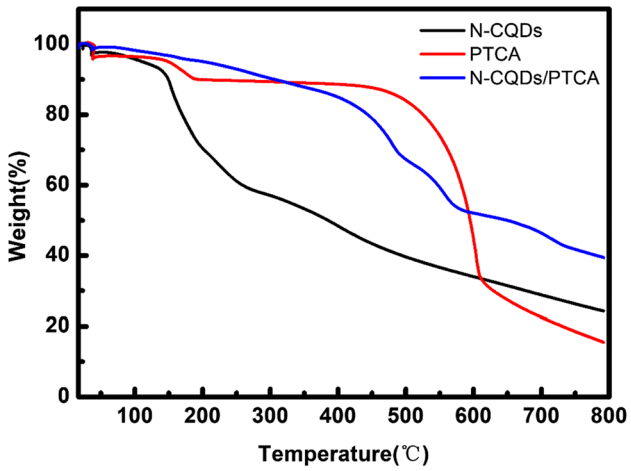

Fig. 5 TGA curve analysis of N-CQDs, PTCA, and N-CQDs/PTCA

In order to evaluate the specificity of the N-CQDs/PTCA fluorescence sensor for detecting metal ions, under the same conditions, one metal cation was added to the N-CQDs/PTCA sensor. F and F_0 indicate the fluorescence intensity of N-CQDs/PTCA in the presence and absence of interfering ions. Usually, we use the ratio of F/F_0, which is the relative fluorescence intensity, to evaluate the degree of influence of interfering ions on the sensing system and the degree of quenching of fluorescence by certain specific response ions. Figure 7a clearly shows that under the same metal ion concentration of 30 μM, the F/F_0 ratio does not change significantly after adding Li^+, Ba^{2+}, Ca^{2+}, Cd^{2+}, K^+, Mg^{2+}, Na^+, Zn^+, and Mn^{2+}. However, in the presence of Fe^{3+}, the degree of fluorescence quenching is significantly different. It can be seen from the value of F/F_0 that Fe^{3+} has the strongest fluorescence quenching ability for N-CQDs/PTCA. It can also be seen from the picture of the N-CQDs/PTCA aqueous solution under the inset ultraviolet lamp in Fig. 7c that the strong green fluorescence of N-CQDs/PTCA is effectively quenched by Fe^{3+} through the charge transfer mechanism. The result of metal–ligand coordination and electrostatic interaction between groups (–COOH, –NH, –OH) can be beneficial to detection. As shown in the mechanism diagram (Fig. 8), Fe^{3+} can coordinate with –COOH, $–NH_2$, –OH, and other groups on the surface of N-CQDs /PTCA and lead to fluorescence quenching by electrostatic interaction. Therefore, N-CQDs/PTCA can be used as a fluorescence detection probe for Fe^{3+}. Figure 7b is a graph of the relationship between the fluorescence intensity obtained after adding different concentrations of Fe^{3+} to the N-CQDs/PTCA. It can be observed that as the concentration of Fe^{3+} increases from 0 to 150 μM, the fluorescence intensity of N-CQDs/PTCA gradually decreases, resulting in complete quenching. It can be seen from Fig. 7d that in the concentration range of 20–60 μM, F_0/F has a good linear relationship with Fe^{3+} concentration. The linear regression equation is $y = 0.02101x + 0.61099$, $R^2 = 0.98268$, where y represents the fluorescence quenching efficiency of N-CQDs/PTCA, and x represents the concentration of Fe^{3+}. Based on the above results, we calculated that when the signal-to-noise ratio is **3**, the lowest detection limit is 0.041 μM. This value is calculated by the formula LOD = 3 σ/k. The analytical parameters were comparable with or even better than most reported fluorescence analytical method for Fe^{3+} ions detection [35, 37–40] (Table 1). The results show that the fluorescence probe based on N-CQDs/PTCA can be used for the determination of heavy metal Fe^{3+}.

The incubation time has a significant effect on the fluorescence quenching efficiency of the N-CQDs/PTCA-Fe^{3+} system. Therefore, we set here six time periods of 0, 1, 2, 5, 10, and 15 min to evaluate the optimal incubation time. It can be seen from Fig. 9a that the quenching efficiency increases rapidly at 1 min, while the quenching efficiency remain unchanged at 2 min, 5 min, and 10 min, and there is no significant change even in the quenching efficiency at 15 min. Therefore, in order to save time, 1 min is chosen as the optimal incubation time, and this time will be used in subsequent experiments. Figure 9b shows the changes in the

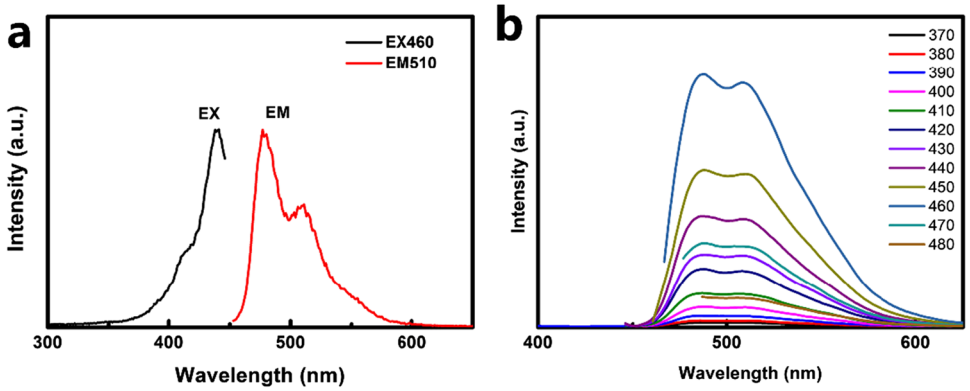

Fig. 6 **a** The maximum PL excitation and emission spectra of N-CQDs/PTCA aqueous solution; **b** the PL emission spectra were obtained under the condition that the excitation wavelength was gradually increased from 370 to 480 nm

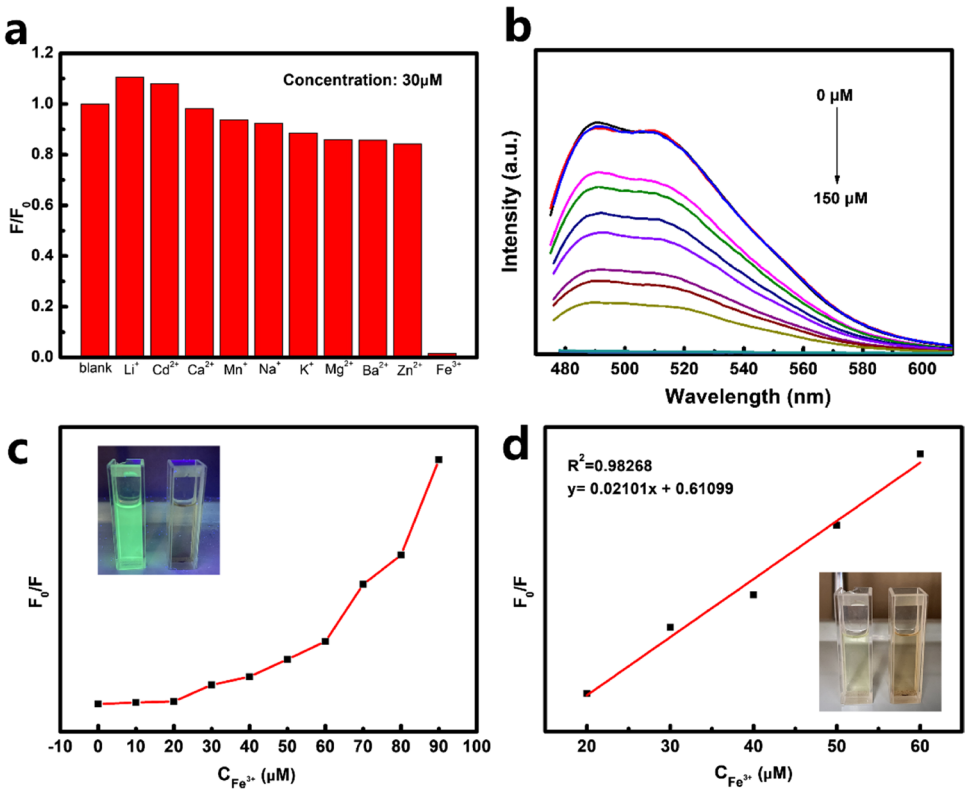

Fig. 7 **a**F/F_0 value of N-CQDs/PTCA aqueous solution at a maximum excitation wavelength of 460 nm in the presence of various metal ions of 30 μM; **b** N-CQDs/PTCA fluorescence spectra after adding different concentrations of Fe^{3+}; **c** with the increase of Fe^{3+} concentration, the fluorescence quenching efficiency of N-CQDs/PTCA (illustration: shows photos of N-CQDs/PTCA with Fe^{3+} and N-CQDs/PTCA without Fe^{3+} under a 365-nm UV lamp). **d** The linear relationship between F_0/F and Fe^{3+} at a concentration of 20–60 μM (illustration: N-CQDs/PTCA and N-CQDs/PTCA photos after adding Fe^{3+})

fluorescence intensity of N-CQDs/PTCA with different pH values at room temperature. It can be clearly observed that the fluorescence intensity will be greatly reduced when the pH value is between 1 and 4, which means that under strong acid conditions, the fluorescence will be quenched. Rather, the fluorescence intensity basically remains unchanged when the pH value is between 5 and 12. These results indicate that the fluorescence of N-CQDs/PTCA may be affected in a strong acid or alkali environment. The effect of different pH values on the fluorescence intensity of N-CQDs/PTCA is due to its own surface groups. Under different pH conditions, the stability of –OH, –NH, and other functional groups on the surface of N-CQDs/PTCA changes, making these functional groups protonated or deprotonation, but only the charge transfer occurs on the surface of the carbon quantum dots, and the core structure is still stable, indicating that N-CQDs/PTCA does not depend on pH. However, under strong acid and alkali conditions, the surface effect has an impact on the stimulated emission transition efficiency of N-CQDs/PTCA, and ultimately leads to changes in the fluorescence intensity of N-CQDs/PTCA.

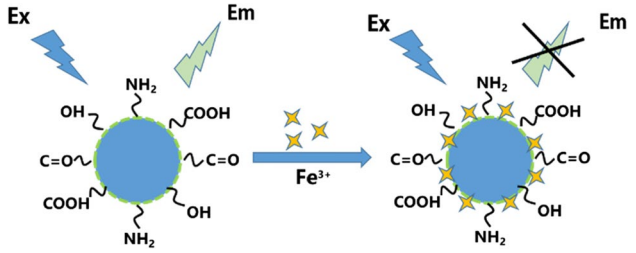

Fig. 8 Mechanism of the fluorescence quenching of N-CQDs/PTCA by Fe^{3+}

Determination of real samples

In order to further confirm the feasibility of the synthetic N-CQDs/PTCA as a fluorescence probe for the detection of

Table 1 Comparison of different fluorescent probe for Fe^{3+} detection

Fluorescent probe	LOD (μM)	Linear range (μM)	Application	Ref
N-L-CQDs	0.48	0–500	Deionized water	[35]
N-CQDs	0.74	3.3–32.2	Deionized water	[37]
Phe-CDs	0.72	5.0–500	Deionized water	[38]
CQDs	0.80	2.5–30	Deionized water	[39]
N-CQDs	1.20	1–1000	Deionized water	[40]
N-CQDs/PTCA	0.41	20–60	This work	

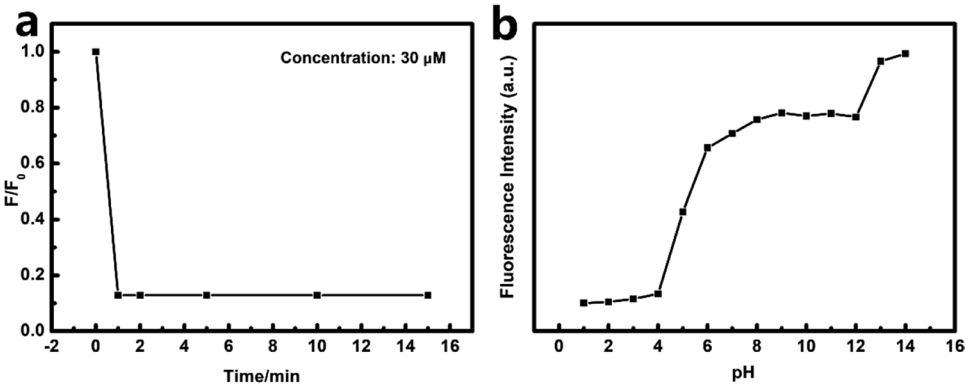

Fig. 9 **a** After adding 30 μM Fe^{3+}, the influence of different incubation time on the fluorescence intensity of N-CQDs/PTCA (the incubation time selected here are respectively 0, 1, 2, 5, 10, and 15 min). **b** The fluorescence intensity of N-CQDs/PTCA aqueous solution at 460 nm under different pH values

Fe^{3+}, we tested two water samples from real environment, tap water and Yellow River water. The recovery rate of Fe^{3+} was obtained by using the standard addition test, and the results are listed in Table 2. It can be seen from Table 2 that the recovery of Fe^{3+} in tap water and Yellow River water is between 97 and 112%, and the RSD is between 2.3 and 5.1%.The results show that the fluorescence sensor based on N-CQDs /PTCA has potential application value for the detection of Fe^{3+} in the real environment. Therefore, we can popularize this fluorescent probe to detect Fe^{3+} in real water samples.

Conclusion

In short, we developed a synthesis process with low synthesis cost, environmental protection, mild reaction conditions, and low consumption. Using citric acid and urea as raw materials, we successfully synthesized nitrogen-doped carbon quantum dots by a simple one-step hydrothermal method. In order to solve the agglomeration effect of carbon quantum dots and increase their recognition sites, nitrogen-doped carbon quantum dots and PTCA with fluorescence properties were combined together to form N-CQDs/PTCA with strong fluorescence. Characterization methods such as FT-IR, XRD, and XPS have proved that they are successfully combined together. Moreover, due to the combination of PTCA, the luminescence behavior of N-CQDs/PTCA is more excellent and independent of the excited wavelength, and bright yellow-green fluorescence can be seen under the ultraviolet lamp. Among the many metal ions, N-CQDs/PTCA has rapid response to Fe^{3+} with a detection limit of 0.041 μM, which shows that N-CQDs/PTCA has very high selectivity and sensitivity to heavy metal Fe^{3+}, and it can be successfully applied to the detection of real water samples. Because Fe^{3+} has a very obvious fluorescence quenching effect on N-CQDs/PTCA, it has the advantages of fast response speed and wide linear range. Therefore, N-CQDs/PTCA can be used as an outstanding fluorescence probe to detect the presence of Fe^{3+}. In addition, because the synthetic method of N-CQDs/PTCA has the advantages of simplicity, speed, time saving, and cost saving, it can also have very broad application prospects in the fields of bioimaging, drug delivery, photocatalysis, and optoelectronic devices.

Table 2 Determination of Fe^{3+} in real samples ($n=5$)

Sample	Original samples	Added (μM)	Founded (μM)	RSD (%)	Recovery (%)
Tap water	Not found	0.5	0.49 ± 0.003	3.2	98 ± 0.3
	Not found	1.0	0.97 ± 0.023	2.3	97 ± 2.3
	Not found	10.0	10.34 ± 0.46	2.9	103.4 ± 4.6
		50.0	51.2 ± 1.71	3.8	102.4 ± 3.42
The Yellow River water	Not found	0.5	0.51 ± 0.009	2.5	102 ± 1.8
	Not found	1.0	1.06 ± 0.052	3.9	106 ± 5.2
	Not found	10.0	11.2 ± 0.51	5.1	112 ± 5.1
	Not found	50.0	53.1 ± 1.30	4.3	106.2 ± 2.6

Content of Fe^{3+} in the sample.

Funding This work was supported by the National Nature Science Foundations of China (Grants no. 21867015, 22065021), the Province Nature Science Foundations of Gansu (Grants no. 20JR5RA453), and Hongliu Outstanding Youth Teacher Cultivate Project of Lanzhou University of Technology.

Declarations

Conflict of interest The authors declare no competing interests.

References

1. Xia C, Zhu S, Feng T, Yang M, Yang B. (2019). Evolution and synthesis of carbon dots: from carbon dots to carbonized polymer dots. Adv Sci 6(23):1901316
2. Gao X, Du C, Zhuang Z, Chen W (2016). Carbon quantum dot-based nanoprobes for metal ion detection. J Mater Chem C 4(29):6927–6945
3. Li X, Zhao S, Li B (2020) Advances and perspectives in carbon dot-based fluorescent probes: mechanism, and application. Coordin Chem Rev 431:213686
4. Bhatt M, Bhatt S, Vyas G (2020) Water-dispersible fluorescent carbon dots as bioimaging agents and probes for Hg^{2+} and Cu^{2+} ions. ACS Appl Nano Mater 3(7):7096–7104
5. Li H, Peng W, Feng W (2016) A novel dual-emission fluorescent probe for the simultaneous detection of H_2S and GSH. Chem Commun 52(25):4628–4631
6. Xu F, Tang H, Yu J (2020) A Cu^{2+}-assisted fluorescence switch biosensor for detecting of coenzyme A employing nitrogen-doped carbon dots. Talanta 224:121838
7. Liu Wen, Zhang R, Kang Y (2019) Preparation of nitrogen-doped carbon dots with a high fluorescence quantum yield for the highly sensitive detection of Cu^{2+} ions, drawing anti-counterfeit patterns and imaging live cells. New Carbon Mater 34(4):390–402
8. Karakoçak BB, Laradji A, Primeau T, Berezin MY, Li S, Ravi N (2020) Hyaluronan-conjugated carbon quantum dots for bioimaging use. ACS Appl. Mater Inter 13(1):277–286
9. Pandey S, Bodas D (2020) High-quality quantum dots for multiplexed bioimaging: A critical review. Adv Colloid Inter 278:102137
10. Wang R, Lu K-Q, Tang Z-R (2017) Recent progress in carbon quantum dots: synthesis, properties and applications in photocatalysis. J Mater Chem A 5(8):3717–3734
11. Feng T, Zeng Q, Lu S (2018) Color-tunable carbon dots possessing solid-state emission for full-color light-emitting diodes applications. ACS Photonics 5(2):502–510
12. Zheng M, Liu S, Li J (2014) Integrating oxaliplatin with highly luminescent carbon dots: an unprecedented theranostic agent for personalized medicine. Adv Mater 26(21):3554–3560
13. Loo AH, Sofer Z, Bouša D, Ulbrich P, Bonanni A, Pumera M (2016) Carboxylic carbon quantum dots as a fluorescent sensing platform for DNA Detection. ACS Appl Mater Inter 8(3):1951–1957
14. Hentze MW, Muckenthaler MU, Galy B (2010) Two to tango: regulation of Mammalian iron metabolism. Cell 142(1):24–38
15. Hsu P-C, Chang H-T (2012) Synthesis of high-quality carbon nanodots from hydrophilic compounds: role of functional groups. Chem Comun 48(33):3984–3986
16. Dalin S, Yan (2010) Effect of ocean acidification on iron availability to marine phytoplankton. Science 327(5966):676–679
17. Abdelhamid HN, Bermejo-Gómez A, Martín-Matute B (2017) A water-stable lanthanide metal-organic framework for fluorimetric detection of ferric ions and tryptophan. Microchim Acta 184(9):3363–3371
18. Qu K, Wang J, Ren J (2013) Carbon dots prepared by hydrothermal treatment of dopamine as an effective fluorescent sensing platform for the label-free detection of iron(III) ions and dopamine. Chem-Eur J 19(22):7243–7249
19. Kim YW, Lee SM, Shin SM (2009) Efficacy of sauchinone as a novel AMPK-activating lignan for preventing iron-induced oxidative stress and liver injury. Free Radical Bio Med 47(7):1082–1092
20. Liu P, Borrell P F, Kokol V (2015) Nanocelluloses and their phosphorylated derivatives for selective adsorption of Ag^{+}, Cu^{2+} and Fe^{3+} from industrial effluents. J Hazard Mater 294:177–185
21. Pati PB, Zade SS (2014) MLCT based colorimetric probe for iron having D-A–D type architecture of benzo[2,1,3]thiadiazole acceptor and thiophene donor with azomethine pendant arm. Inorg Chem Commun 39:114–118
22. Rain UA, Ng LY, Ng CY (2020) A review of carbon quantum dots and their applications in wastewater treatment. J Colloid Interf Sci 278:1021
23. Walther B K, Dinu C Z, Guldi D M (2020) Nanobiosensing with graphene and carbon quantum dots: recent advances. Mater Today 39:23–46
24. Qin K, Zhang D, Ding Y (2020) Applications of hydrothermal synthesis of Escherichia coli derived carbon dots in in vitro and in vivo imaging and p-nitrophenol detection. Analyst 145(1):177–183
25. Saravanan A, Maruthapandi M, Das P (2020) Applications of N-doped carbon dots as antimicrobial agents, antibiotic carriers, and selective fluorescent probes for nitro explosives. ACS Appl Bio Mater 3(11):8023–8031
26. Liu Z, Chen M, Guo Y (2020) Oxidized nanocellulose facilitates preparing photoluminescent nitrogen-doped fluorescent carbon dots for Fe^{3+} ions detection and bioimaging. Chem Eng J 384:123260
27. Peng B, Fan M, Xu J (2020) Dual-emission ratio fluorescent probes based on carbon dots and gold nanoclusters for visual and fluorescent detection of copper ions. Microchim Acta 187(12):1–9
28. Xiao H, Li P, Tang B (2021) Recent progresses in fluorescent probes for detection of polarity. Coordin Chem Rev 427:213582
29. Pang S, Liu S (2020) Dual-emission carbon dots for ratiometric detection of Fe^{3+} ions and acid phosphatase. Anal Chim Acta 1105:155–161
30. Song Z, Chen X, Gong X (2020) Luminescent carbon quantum dots/nanofibrillated cellulose composite aerogel for monitoring adsorption of heavy metal ions in water. Opt Mater 100:109642
31. Li J, Shan X, Jiang D (2020) A novel electrochemiluminescence sensor based on resonance energy transfer from MoS2QDs@g-C3N4 to NH2-SiO2@PTCA for glutathione assay. Analyst 145(23):7616–7622
32. Yang T, Cui Y, Li Z (2018) Enhancement of the corrosion resistance of epoxy coating by highly stable 3, 4, 9, 10-perylene tetracarboxylic acid functionalized graphene. J Hazard Mater 357:475–482
33. Goswami T, Bheemaraju A, Kataria A (2021) Highly fluorescent water-soluble PTCA incorporated silver nano-cluster for sensing of dopamine. Mater Chem Phys 259:124086
34. Petzel-Witt S, Meier SI, Schubert-Zsilavecz M (2018) PTCA (1H-pyrrole-2, 3, 5-tricarboxylic acid) as a marker for oxidative hair treatment. Drug Test Anal 10(4):768–773
35. Jiang X, Shi Y, Liu X, Wang M, Song P, Xu F, Zhang X (2018) Synthesis of Nitrogen-doped lignin/DES carbon quantum dots as a fluorescent probe for the detection of Fe^{3+} ions. Polymers 10(11):1282

36. Wu S, Li W, Sun Y, Zhang X (2019) Synthesis of dual-emissive carbon dots with a unique solvatochromism phenomenon. J Colloid Interf Sci 555(2019):607–614
37. Qi H, Teng M, Liu M (2019) Biomass-derived nitrogen-doped carbon quantum dots: highly selective fluorescent probe for detecting Fe^{3+} ions and tetracyclines. J Colloid Interf Sci 539:332–341
38. Pu Z-F, Wen Q-L, Yang Y-J (2020) Fluorescent carbon quantum dots synthesized using phenylalanine and citric acid for selective detection of Fe^{3+} ions. Sprctrochim Acta A 229:117944
39. Wang Y, Lao S, Ding W, Zhang Z, Liu S (2019) A novel ratiometric fluorescent probe for detection of iron ions and zinc ions based on dual-emission carbon dots. Sensor Actuat B-Chem 284:186–192
40. Atchudan R, Jebakumar Immanuel Edison TN, Perumal S, Lee YR (2018) Indian gooseberry-derived tunable fluorescent carbon dots as a promise for in vitro/in vivo multicolor bioimaging and fluorescent ink. ACS Omega 3(12):17590–17601